
12 Aug 2020

Factorization of High-Order-Harmonic-Generation Yields in Impurity-Doped Materials

Van Hung Hoang

Anh-Thu Le

Missouri University of Science and Technology, lea@mst.edu


Follow this and additional works at: https://scholarsmine.mst.edu/phys_facwork

 Part of the [Physics Commons](#)

Recommended Citation

V. H. Hoang and A. Le, "Factorization of High-Order-Harmonic-Generation Yields in Impurity-Doped Materials," *Physical Review A*, vol. 102, no. 2, American Physical Society, Aug 2020.
The definitive version is available at <https://doi.org/10.1103/PhysRevA.102.023112>

This Article - Journal is brought to you for free and open access by Scholars' Mine. It has been accepted for inclusion in Physics Faculty Research & Creative Works by an authorized administrator of Scholars' Mine. This work is protected by U. S. Copyright Law. Unauthorized use including reproduction for redistribution requires the permission of the copyright holder. For more information, please contact scholarsmine@mst.edu.

Factorization of high-order-harmonic-generation yields in impurity-doped materialsVan-Hung Hoang ^{1,2,3,*} and Anh-Thu Le¹¹*Department of Physics, Missouri University of Science and Technology, Rolla, Missouri 65409, USA*²*Atomic Molecular and Optical Physics Research Group, Advanced Institute of Materials Science, Ton Duc Thang University, Ho Chi Minh City, Vietnam*³*Faculty of Applied Sciences, Ton Duc Thang University, Ho Chi Minh City, Vietnam*

(Received 31 March 2020; revised 28 June 2020; accepted 24 July 2020; published 12 August 2020)

We present a theoretical investigation of high-order-harmonic generation (HHG) from impurity-doped materials. Based on the analysis of the exact numerical solutions of the time-dependent Schrödinger equation (TDSE) for one-dimensional models, we demonstrate the factorization of HHG yields as a product of an electron wave packet and the recombination cross section, in analogy to HHG from atoms and molecules in the gas phase. Furthermore, we show that the quantitative rescattering model based on this factorization accurately reproduces the TDSE results. This opens up new possibilities to study impurities in materials using the available techniques from strong-field physics.

DOI: [10.1103/PhysRevA.102.023112](https://doi.org/10.1103/PhysRevA.102.023112)**I. INTRODUCTION**

High-order-harmonic generation (HHG) from atoms and molecules in gas phase is one of the most important phenomena in intense laser-matter interactions. It provides not only table-top coherent XUV to soft-x-ray light sources, but also a powerful technique to produce attosecond pulses for applications in science and technology [1]. It has been studied over the last three decades and the mechanism behind HHG in gases is now well understood based on the three-step recollision model [2,3]. Only recently, HHG in solids was demonstrated experimentally with midinfrared [4–6], visible [7], and terahertz lasers [8,9]. The recollision was also found to be responsible for a related process of high-order-sideband generation using terahertz lasers [10]. Subsequently, HHG has been observed in a variety of materials, including wide band-gap dielectrics [11–13], amorphous common glass [14], and graphene [15]. Recently, improvements of the recollision model in HHG from solids have been reported [16,17]. Due to their high atomic density, it has been expected that solids have the potential to produce more efficient HHG, as compared to atoms and molecules in the gas phase.

Quite recently, it was demonstrated both experimentally and theoretically that HHG from solids can be enhanced if the material is doped by impurities [6,18–21]. In fact, impurities or target engineering in general are typically used to alter the band structures of a solid, therefore allowing one to actively control various processes in the material. Conceptually, it was shown that the three-step recollision model can be extended for HHG from impurities in solids [19,20]. This indicates that the HHG process from impurities in solids is very similar to that from gases.

In this paper we show that HHG yields from impurities can be expressed as a product of a returning electron wave packet and the photorecombination cross section for electrons in conduction bands back to the impurity ground state. This indicates that the quantitative rescattering theory (QRS) for atoms and molecules in the gas phase [22–27] can be extended to HHG from impurities in solids. Our results therefore confirm the validity of the three-step model and recollision picture for HHG from impurities [19,20] and elevate it to a more quantitative level.

II. THEORETICAL METHODS

To simulate a HHG process, we solve the time-dependent Schrödinger equation (TDSE) for solids in an intense laser pulse within the single-active-electron approximation (SAE). This approach has been used by different groups [28–36]. Electron correlation has typically been taken into account empirically via dephasing times in the semiconductor Bloch equations (SBEs) approach [28,37–39]. To reproduce typical “clean” experimental spectra, a small dephasing time of the order of 1 fs has been used. Note that an approach based on the solution of the time-dependent density functional theory (TDDFT) has also been used, in which the electron exchange and correlation can be taken into account [20,39–42]. However, it was shown that within the TDDFT the spectra are quite noisy [39,40], although the results agree well with the SBEs when a large dephasing time is used. Furthermore, it was shown that the use of the frozen Kohn-Sham potential leads to quite similar results as of the full TDDFT calculations. An attempt to treat electron correlation was also reported for HHG in a strongly correlated system [43]. We remark that the adequacy and limitations of the SAE approximation have been addressed recently [35]. They pointed out that the SAE model agrees well with the SBEs approach if contributions from all the states in the valence band (VB) are taken into account in

*hoangvanhung@tdtu.edu.vn

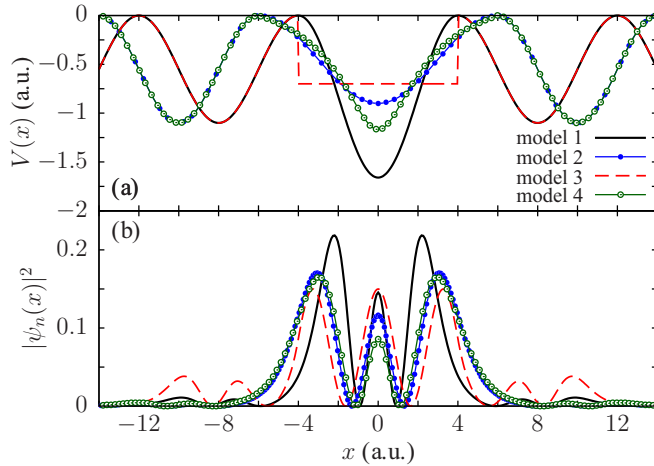


FIG. 1. The model potentials used in this paper (a) and the probability density of the impurity ground-state orbitals for four models (b). The results are shown near the doping site, chosen to be at $x = 0$.

the SAE and when the dephasing time in the SBEs is relatively large.

We model the undoped solid as a linear chain of N atoms located with a separation a_0 . The effective potential for the active electron inside the undoped solid is modeled by a Mathieu-type potential as (atomic units are used throughout this paper, unless otherwise indicated)

$$v(x) = -v_0[1 + \cos(2\pi x/a_0)]. \quad (1)$$

In this paper we choose $N = 101$, $v_0 = 0.55$, and the lattice constant $a_0 = 8$. This model potential has been used by different groups [18,31,32]. For the doped materials, we consider the case when dopant atoms substitute atoms of the undoped solid. To describe the effect of different impurity species on HHG spectra, we use four different model potentials for $v(x)$ near the doping site. We have limited ourselves to simple model potentials in order to illustrate the main physics. To be specific, we choose the doping site to be at $x = 0$. This means that the doping rate is 1%. As compared to the undoped case, the model potential is assumed to be modified only in the region close to the impurity atom with $|x| \leq a_1/2$. In this region, we use Mathieu-type potential

$$v(x) = -v_1[1 + \cos(2\pi x/a_1)] \quad (2)$$

with parameters $v_1 = 0.83$ and $a_1 = 8$ and $v_1 = 0.45$ and $a_1 = 12$ for model 1 and 2, respectively. For model 3, we use $v(x) = -v_1$ with $v_1 = 0.7$ and $a_1 = 8$ for $|x| \leq a_1/2$. For model 4 we use

$$v(x) = -\frac{v_1}{\sqrt{x^2 + 3}} + \frac{v_1}{\sqrt{(a_1/2)^2 + 3}}, \quad (3)$$

with $v_1 = 2.8$ and $a_1 = 12$. The four model potentials near the impurity are shown in Fig. 1(a).

The time-independent Schrödinger equation can be written as

$$\hat{H}_0 \psi_n(x) = E_n \psi_n(x), \quad (4)$$

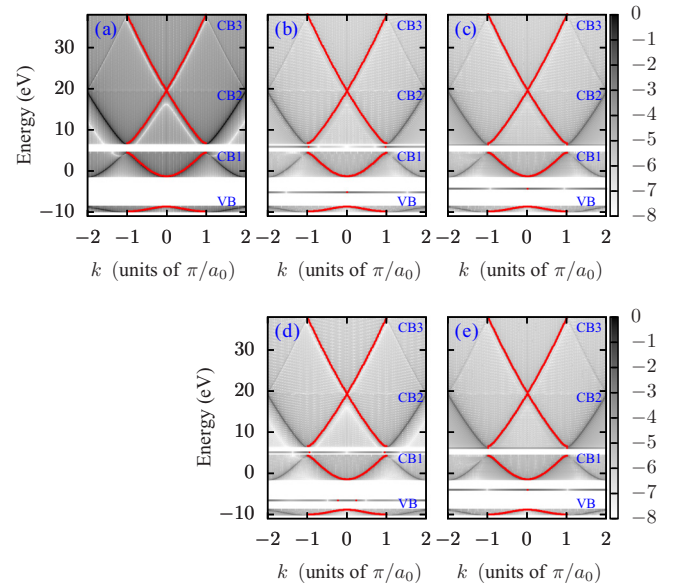


FIG. 2. Band structures of the undoped solid (a) and doped solids with model 1 (b), 2 (c), 3 (d), and 4 (e), as given by the probability densities for the eigenstates of \hat{H}_0 in the momentum space. The maximum of the probability densities for each energy is shown by a red dot. In (b)–(e), the isolated horizontal lines correspond to the impurity orbitals. The bands below the top valence band are not shown, since they practically are not involved in HHG process.

where $\hat{H}_0 = \hat{p}^2/2 + v(x)$. The above equation is solved by the discrete variable representation method with a uniform grid in the basis of Fourier functions [44]. For $N = 101$ atoms and the lattice constant $a_0 = 8$ a.u., we use the box size of $[-404 : 404]$ a.u. Following Refs. [42,45], we calculate the band structures using the spatial Fourier transforms of the eigenfunctions of Hamiltonian H_0 . This is illustrated in Figs. 2(a)–2(e) for the undoped and doped solids with model 1, 2, 3, and 4, respectively, where the probability densities in the momentum space (k space) are plotted at their respective energies on a logarithmic scale. To verify the results, we also calculated the band structure of the undoped solid using the Bloch state basis. The two results are identical. At such a low doping rate (1%), the band structures do not change much and the impurity states are energetically isolated. This is consistent with the earlier results [20], in which the density-functional theory was used.

In all four cases, there is an isolated energy level around -5 eV, i.e., in between the VB and the first conduction band (CB1). Clearly, this energy level is associated with an impurity state. Within the single-active-electron model, we choose to associate this state with the highest occupied orbital of the impurity atom, which will also be called the impurity “ground” state for simplicity in the following. The probability densities of the impurity ground states for the four models are shown in Fig. 1(b). Clearly, the impurity wave functions are mostly localized around the impurity site. Since the energy gap between the the impurity ground state and CB1 is much smaller than the band gap between the VB and CB1, it is expected that the HHG yields from doped solids in all four cases are significantly stronger than that from the undoped

material. Our calculations based on the solutions of the TDSE indeed confirmed this expectation, in general agreements with results based on the TDDFT for donor-doped materials [20].

The time-dependent Hamiltonian for the doped material interacting with an intense laser pulse polarized along the x axis can be written in the length gauge within the dipole approximation as

$$\hat{H} = \hat{H}_0 + xE(t), \quad (5)$$

where the laser pulse is given by

$$E(t) = E_0 \cos^2\left(\frac{\pi t}{\tau}\right) \cos(\omega_0 t + \varphi) \quad (6)$$

for the time interval $(-\tau/2, \tau/2)$ and zero elsewhere. Here E_0 is the laser peak electric-field amplitude, ω_0 is the carrier frequency, and φ is the carrier-envelope phase. For this choice of laser envelope, the pulse duration, defined as the full width at half maximum of the intensity, is given as $\Gamma = \tau/2.75$.

The TDSE with Hamiltonian (5) is solved by the split-operator method with the impurity ground-state wave function taken as the initial wave function. To avoid the unphysical reflection due to a finite box size, we use an absorbing boundary of the form of $\cos^{1/4}$. The numerical calculations are performed on a uniform spatial grid with $\Delta x = 0.1$ and a time step $\Delta t = 0.2$. We have checked these parameters to make sure that converged results were obtained. Once the time-dependent wave function is obtained, the time-dependent laser-induced currents $j(t)$ can be calculated. The HHG spectrum is then given as the modulus square of the Fourier transform of time-dependent laser-induced currents, where a window function $\cos^8(\frac{\pi t}{\tau})$ has been applied before the Fourier transform is carried out [46]. We have also found that identical spectra are obtained by using the laser-induced dipoles.

III. RESULTS AND DISCUSSION

A. Enhancement of HHG yields in donor-doped models

Before presenting our main results, we remark that in this paper we only consider the case of donor-type doping. Within the SAE model this means that the impurity orbital with energy near -5 eV is occupied, as discussed above. In the case of acceptor-type doping, that impurity orbital is unoccupied. As reported in Ref. [20], a donor-doped material can enhance HHG yields by several orders of magnitude. Furthermore, they showed that the enhancement was mainly due to the contribution from the highest occupied orbital alone, which is the orbital of the impurity. Our calculations based on the SAE model generally confirm that finding. Within the SAE model for the impurity-doped solid the initial state is chosen to be the impurity ground state. For the undoped solid, previous works showed that only the VB contributes, with the dominant contribution from the state on the top of the VB. In fact, except for a few cases [20,34], the majority of the works have only focused on the contribution from this state. In that case, the initial state was chosen to be the state on the top of the VB. In principle, the induced dipoles from other states in the VB can be calculated in the same manner. The total induced dipole is then obtained by adding up all the contributions coherently. We note in passing that HHG from acceptor-type doped solids was also reported in Refs. [18,20].

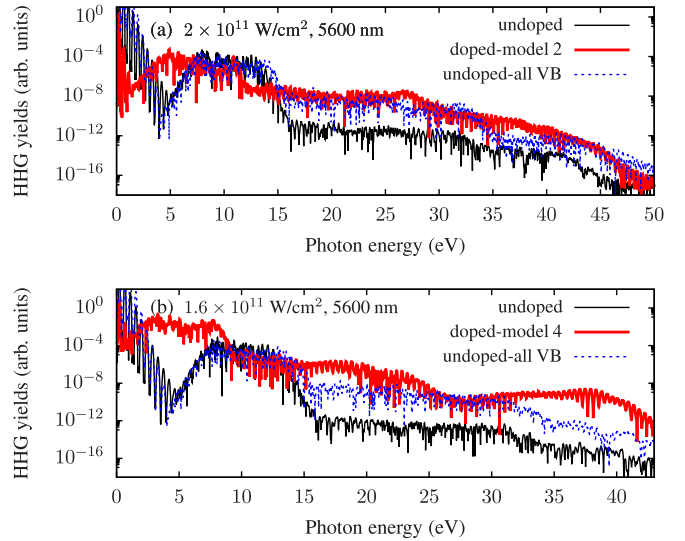


FIG. 3. (a) Comparison of HHG spectra from the undoped and impurity-doped (with model 1) solids. The results were obtained from the TDSE with ten-cycle laser pulse at wavelength of $5.6 \mu\text{m}$ and intensity of $2 \times 10^{11} \text{ W/cm}^2$. (b) Same as in (a), but for model 4 at the laser intensity of $1.6 \times 10^{11} \text{ W/cm}^2$.

For illustration, we show in Fig. 3(a) the comparison of the HHG spectra from the undoped and impurity-doped (1% doping, with model 1) solids. The results were obtained from the TDSE with a ten-cycle laser pulse at wavelength of $5.6 \mu\text{m}$ and intensity of $2 \times 10^{11} \text{ W/cm}^2$. For the contribution from the highest occupied orbital, an enhancement of about five orders of magnitude can be seen for energies above 15 eV. This is in general agreement with the previous finding [20,36]. Our calculations also show that, although the contribution from each of the lower states in the VB decreases as its energy gap with the CB increases, the total contribution from the whole VB is quite comparable with that from the impurity alone. This is somewhat different from the TDDFT results by Yu *et al.* [20]. Nevertheless, the significant contribution from the lower states in the VB is in a good agreement with Navarrete *et al.* [34], who used the Kronig-Penney model instead of the Mathieu-type potential. It is possible that the SAE model overestimates the total yields from the VB, since the active electron is allowed to populate the other states in the VB during the laser pulse, even though these states are occupied by other electrons. This effect is negligible for the impurity state since it is energetically well separated from the neighboring states.

Similar enhancements were found for other impurity models considered in this paper. As another illustration, we show in Fig. 3(b) a comparison for model 4 at the laser intensity of $1.6 \times 10^{11} \text{ W/cm}^2$. In this case, the HHG from impurities largely dominates over the HHG from the whole VB, except for the energies near 12 and 27 eV, where they are comparable. Again, we see that the HHG from the top of the VB is much weaker than that from the impurities.

We found a rather similar level of enhancement for other laser parameters as well. Clearly, the enhancement can be further increased with a higher doping rate. Therefore in the following we only focus on the HHG from the impurity

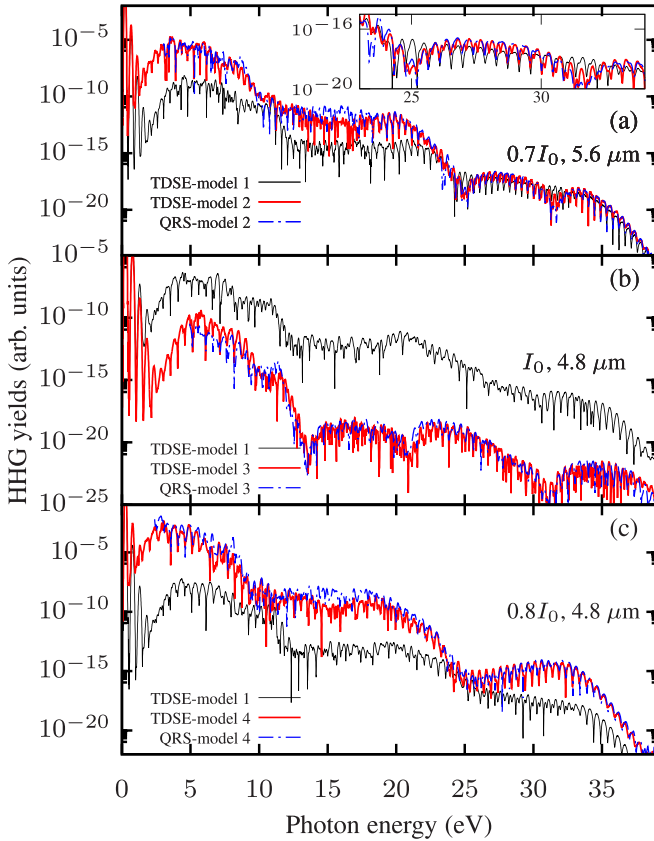


FIG. 4. (a) Comparison of HHG spectra from model 1 and model 2 obtained from the TDSE with the same ten-cycle laser pulse at wavelength of $5.6 \mu\text{m}$ and intensity of $7 \times 10^{10} \text{ W/cm}^2$. The QRS result for model 2 is shown as the dashed line. (b) Same as (a) but for model 1 and 3 for the laser pulse at wavelength of $4.8 \mu\text{m}$ and intensity of 10^{11} W/cm^2 . (c) Same as (a) but for model 1 and 4 for the laser pulse at wavelength of $4.8 \mu\text{m}$ and intensity of $8 \times 10^{10} \text{ W/cm}^2$.

state, assuming that the HHG contribution from the VB1 can largely be neglected for the donor-type doping with a sufficient doping rate of a few percent.

B. Analysis of HHG spectra: Main features and their origins

In the following, we will use model 1 as a reference system for comparison with the other models. In Fig. 4(a) we compare HHG spectra obtained from the TDSE for model 1 and model 2 under the same ten-cycle laser pulse at wavelength of $5.6 \mu\text{m}$ and intensity of $7 \times 10^{10} \text{ W/cm}^2$. There are three distinct energy regions (or plateaus) above the threshold at about 5 eV. By comparing with Fig. 2, the first plateau (from 5 eV to about 10 eV) can be associated with the recombination from CB1 back to the impurity ground state. Similarly, the second and third plateau, from 13 to 22 eV and from 25 to 35 eV, respectively, is associated with the recombination from CB2 and CB3 to the impurity, respectively. For each model, there are significant drops in HHG yields for energy regions between the plateaus. This can be attributed to the exponential decrease of excitation from a lower conduction band to the next one. Note that the first plateau in model 1 is slightly more extended than that of model 2. This is due to the presence of

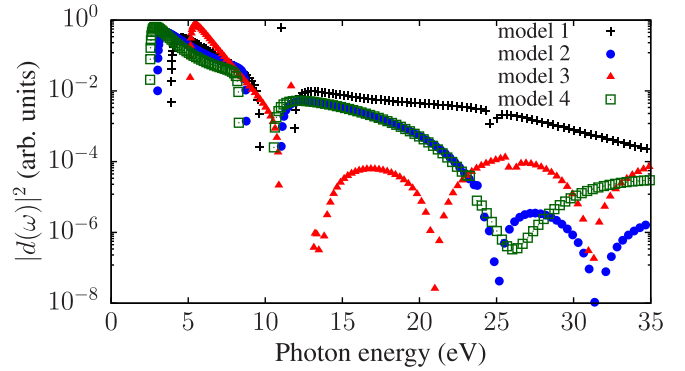


FIG. 5. Modulus squared of transition dipoles from the impurity ground state to the conduction bands vs photon energy for model 1, 2, 3, and 4.

an impurity level in the energy gap between CB1 and CB2 in model 1.

Furthermore, for the harmonics below 20 eV, the HHG yield from model 2 is about two orders of magnitude stronger than that of model 1. This is not entirely surprising, since the energy gap between the highest occupied orbital of the impurity and CB1 in model 2 is about 2 eV smaller (see Fig. 2). However, for the energies above 23 eV, the HHG yields from the two models are nearly identical, except that model 2 shows two minima near 25 and 32 eV while there is no obvious structure in model 1.

To understand the origin of this behavior, we compare in Fig. 5 the modulus square of the transition dipoles from the conduction bands to the impurity ground state for models 1–4, as they are proportional to the photoexcitation and photo-recombination cross sections. For models 1 and 2 in the energy range below 10 eV, the cross sections are quite similar. Therefore the difference in the HHG yields in this energy range from the two models could be attributed mainly to the differences in tunneling excitation (or “ionization”) from the impurity ground state to CB1, which in turn depends on the energy gaps as discussed above. For the energies between 12 and 20 eV, the two cross sections start to deviate from one another and the HHG yields from the two models start to come closer. For the energies above 23 eV, the cross section from model 1 is about two to three orders of magnitude stronger than that of model 2. That somewhat compensates the weaker “ionization” in model 1 so that the HHG yields from the two models are nearly identical above 23 eV. Furthermore, a closer look at the HHG spectrum from model 2 reveals two minima near 25 and 31 eV, at the same energies that its cross section has minima. In contrast, model 1 shows no obvious minimum in that energy range in both HHG and cross section.

Similar comparisons for model 3 and model 4 with model 1 are shown in Figs. 4(b) and 4(c), respectively. The laser parameters are given in the figure caption. Here, the locations of the plateaus are quite similar to that of Fig. 4(a). More importantly, for all the cases, the structures in HHG spectra follow closely the cross sections, shown in Fig. 5. In particular, the pronounced minima in the HHG spectrum for model 3 near 13, 21, and 31 eV are clearly associated with the three minima in the cross sections at the same energies. For

model 4, the broad minimum in the HHG spectrum near 26 eV is caused by the respective minimum in the cross section. Again, there is no obvious minimum in the same energy regions in both HHG and cross section for model 1.

C. The validity of the QRS and the retrieval of the transition dipoles

The above analysis indicates a close relationship between HHG and the transition dipole. In the following we will present the main result of this paper: we will show that the QRS [22–25] can be extended for impurities in solids. According to the QRS theory, HHG yields can be calculated as a product of an electron wave packet $W(\omega)$ and the transition dipole $d(\omega)$ as

$$S(\omega) \propto |W(\omega)d(\omega)|^2, \quad (7)$$

where

$$d(\omega) = \langle \psi_0 | x | \psi_n \rangle, \quad (8)$$

with $\psi_0(x)$ and $\psi_n(x)$ being the wave function of the impurity ground state and a state in the CB, respectively. The emitted HHG photon energy ω is related to the energies of these two states by $\omega = E_n - E_0$.

The above equations are formally the same as in the original QRS which was developed for atoms and molecules in the gas phase. For those targets, the electron returning wave packet $W(\omega)$ can be calculated within certain approximations (for example, the strong-field approximation). It turns out that the wave packets from different targets, as functions of energy, are nearly identical (up to an overall factor), under the same laser parameters. Therefore, for practical applications of the QRS, one can “borrow” the wave packet from a reference system. In fact, assuming that Eq. (7) is valid, the wave packet for the reference target would be $|W^{\text{ref}}(\omega)|^2 \propto S^{\text{ref}}(\omega)/|d^{\text{ref}}(\omega)|^2$. One then uses this wave packet to calculate the HHG spectrum for a new target by using Eq. (7). Results from this procedure will be compared with available the “exact” TDSE or experimental results and good agreements would validate this procedure and the QRS.

Since the conduction bands are not affected much by the presence of the impurities for a relatively low doping rate, one can reasonably expect that the electron wave packets for different impurities under the same laser are nearly identical (up to overall constants, which account for different excitation probabilities from the impurity ground states to the conduction bands). Therefore, by following the above procedure, one can, for example, obtain the HHG spectrum for a target, if a HHG spectrum for a reference target under the same laser is known [22–24]. To be specific, we assume that the QRS can be applied to target 1 and target 2 under the same laser. We then have $S_1(\omega) \propto |W_1(\omega)d_1(\omega)|^2$ and $S_2(\omega) \propto |W_2(\omega)d_2(\omega)|^2$. Since $|W_2(\omega)|^2 = C|W_1(\omega)|^2$, with C being an overall constant, we then have

$$S_2(\omega) = CS_1(\omega) \frac{|d_2(\omega)|^2}{|d_1(\omega)|^2}. \quad (9)$$

HHG spectra obtained with the QRS model are shown in Fig. 4 as dashed lines. In all the cases, they agree very well with the exact TDSE for the whole energy region above the

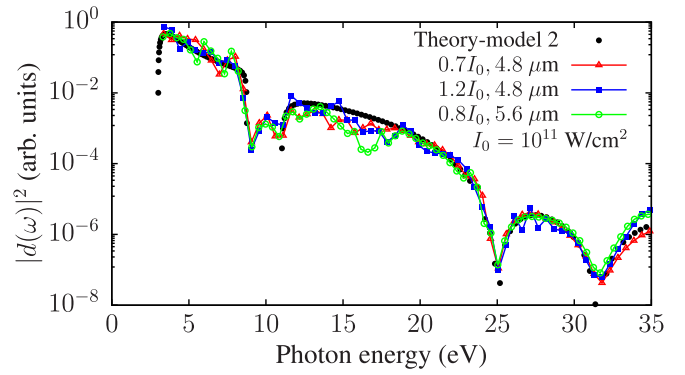


FIG. 6. Retrieved modulus squared of transition dipole from the impurity ground state to the conduction bands vs photon energy for model 2 using HHG with different lasers. The laser parameters are given in the labels. Here, $I_0 = 10^{11}$ W/cm². The theoretical result for the laser-free transition dipole is also shown as black solid dots.

threshold. Here, model 1 was used as the reference target for all the cases.

Using the QRS in the same manner as it is done for gases, one can also extract the transition dipole for an unknown impurities target, if HHG spectra for the target and a reference target under the same laser are known. In fact, Eq. (9) can be written as

$$|d_2(\omega)|^2 = C^{-1}|d_1(\omega)|^2 \frac{S_2(\omega)}{S_1(\omega)}. \quad (10)$$

If the QRS is valid, the retrieved transition dipole would be independent of laser parameters. We show the results for model 2 in Fig. 6. The retrieved transition dipoles squared, obtained from HHG spectra with different lasers, indeed agree well with the theoretical data (black solid dots) for a broad range of energy from the threshold to 35 eV. In particular, the minima near 25 and 32 eV are nicely retrieved. Here, we use model 1 as the reference target.

The above results were obtained under the condition that HHG from the impurities dominates the spectra. It illustrates the level of accuracy the retrieval could achieve in this ideal case. Or one can put it in another way: our method allows us to simulate the contribution from the impurities. In practice, the retrievals need to be checked carefully by varying experimental parameters, including laser intensity and wavelength as well as the doping rate. This would allow experimentalists to assess the quality of the retrieval especially for the energy region where contribution from impurities might not quite dominate. We remark that photoionization cross sections for atoms and molecules in the gas phase have been retrieved experimentally from HHG measurements by using the same method (see, for example, Refs. [47–49]). Quite recently, a tomographic reconstruction of impurity orbitals using HHG was suggested based on the three-step model [19]. Furthermore, it was experimentally demonstrated that the transition dipole moment in momentum space in two-dimensional semiconductors can be probed using polarization-resolved HHG measurements [50].

Our microscopic treatment of HHG needs to be complemented by macroscopic propagation simulations for realistic comparisons with experiments. In principle, this can be done

by solving coupled TDSE and Maxwell's equations. Progress along this direction was reported recently [39].

IV. CONCLUSIONS

In conclusion, we have established that HHG yields from impurities in doped materials can be expressed as a product of an electron wave packet and transition dipole for the electron in a conduction band back to the impurity ground state. This process therefore resembles very closely the HHG process in atoms and molecules in the gas phase, except that the conduction bands now play the role of the continuum. Based on this approximate factorization, we have extended the quantitative rescattering theory for HHG from impurities in solids. We expect that our theory can serve as a simple starting point to study HHG in solids for realistic systems. Research along this direction could provide detailed information about impurities in a solid environment, needed for

understanding and controlling various processes in engineered solid structures. Finally, we remark that the effect of disorder and vacancies on HHG in solids has been reported [42,51–54]. We expect that our approach can be extended to these cases as well.

ACKNOWLEDGMENTS

V.H.H. is funded by the Program of Fundamental Research of Ministry of Education and Training (Vietnam) under Grant No. B2016.19.10, and by the Vietnam National Foundation for Science and Technology Development (NAFOSTED) under Grant No. 103.01-2017.371. The computing part of this project was performed on the Forge cluster at Missouri University of Science and Technology. A.T.L. thanks Lars Bojer Madsen, Chuan Yu, and Kenneth K. Hansen for valuable and insightful discussions. Finally, we thank the referees for helpful suggestions.

-
- [1] F. Krausz and M. Ivanov, *Rev. Mod. Phys.* **81**, 163 (2009).
- [2] P. B. Corkum, *Phys. Rev. Lett.* **71**, 1994 (1993).
- [3] J. L. Krause, K. J. Schafer, and K. C. Kulander, *Phys. Rev. Lett.* **68**, 3535 (1992).
- [4] S. Ghimire, A. D. DiChiara, E. Sistrunk, P. Agostini, L. F. DiMauro, and D. A. Reis, *Nat. Phys.* **7**, 138 (2011).
- [5] G. Vampa, T. J. Hammond, N. Thiré, B. E. Schmidt, F. Légaré, C. R. McDonald, T. Brabec, and P. B. Corkum, *Nature (London)* **522**, 462 (2015).
- [6] M. Sivis, M. Taucer, G. Vampa, K. Johnston, A. Staudte, A. Y. Naumov, D. M. Villeneuve, C. Ropers, and P. B. Corkum, *Science* **357**, 303 (2017).
- [7] T. T. Luu, M. Garg, S. Y. Kruchinin, A. Moulet, M. T. Hassan, and E. Goulielmakis, *Nature (London)* **521**, 498 (2015).
- [8] O. Schubert, M. Hohenleutner, F. Langer, B. Urbanek, C. Lange, U. Huttner, D. Golde, T. Meier, M. Kira, S. W. Koch, and R. Huber, *Nat. Photonics* **8**, 119 (2014).
- [9] M. Hohenleutner, F. Langer, O. Schubert, M. Knorr, U. Huttner, S. W. Koch, M. Kira, and R. Huber, *Nature (London)* **523**, 572 (2015).
- [10] B. Zaks, R. B. Liu, and M. S. Sherwin, *Nature (London)* **483**, 580 (2012).
- [11] G. Ndabashimiye, S. Ghimire, M. Wu, D. A. Browne, K. J. Schafer, M. B. Gaarde, and D. A. Reis, *Nature (London)* **534**, 520 (2016).
- [12] Y. S. You, D. Reis, and S. Ghimire, *Nat. Phys.* **13**, 345 (2017).
- [13] T. T. Luu and H. J. Wörner, *Nat. Commun.* **9**, 916 (2018).
- [14] Y. S. You, Y. Yin, Y. Wu, A. Chew, X. Ren, F. Zhuang, S. Gholam-Mirzaei, M. Chini, Z. Chang, and S. Ghimire, *Nat. Commun.* **8**, 724 (2017).
- [15] N. Yoshikawa, T. Tamaya, and K. Tanaka, *Science* **356**, 736 (2017).
- [16] L. Yue and M. B. Gaarde, *Phys. Rev. Lett.* **124**, 153204 (2020).
- [17] A. M. Parks, G. Ernotte, A. Thorpe, C. R. McDonald, P. B. Corkum, M. Taucer, and T. Brabec, [arXiv:2006.09651](https://arxiv.org/abs/2006.09651).
- [18] T. Huang, X. Zhu, L. Li, X. Liu, P. Lan, and P. Lu, *Phys. Rev. A* **96**, 043425 (2017).
- [19] S. Almalki, A. M. Parks, G. Bart, P. B. Corkum, T. Brabec, and C. R. McDonald, *Phys. Rev. B* **98**, 144307 (2018).
- [20] C. Yu, K. K. Hansen, and L. B. Madsen, *Phys. Rev. A* **99**, 013435 (2019).
- [21] V. E. Nefedova, S. Fröhlich, N. Tancogne-Dejean, W. Boutu, F. Navarrete, M. F. Ciappina, D. Franz, D. Gauthier, A. Hamdou, S. Kaassamani, R. Nicolas, Q. Ripault, G. Jargot, U. Thumm, M. Hanna, P. Georges, A. Rubio, and H. Merdji, [arXiv:2001.00839](https://arxiv.org/abs/2001.00839).
- [22] T. Morishita, A.-T. Le, Z. Chen, and C. D. Lin, *Phys. Rev. Lett.* **100**, 013903 (2008).
- [23] A.-T. Le, R. R. Lucchese, S. Tonzani, T. Morishita, and C. D. Lin, *Phys. Rev. A* **80**, 013401 (2009).
- [24] C. D. Lin, A.-T. Le, Z. Chen, T. Morishita, and R. Lucchese, *J. Phys. B* **43**, 122001 (2010).
- [25] A.-T. Le, H. Wei, C. Jin, and C. D. Lin, *J. Phys. B* **49**, 053001 (2016).
- [26] M. V. Frolov, N. L. Manakov, T. S. Sarantseva, M. Y. Emelin, M. Y. Ryabikin, and A. F. Starace, *Phys. Rev. Lett.* **102**, 243901 (2009).
- [27] M. V. Frolov, N. L. Manakov, T. S. Sarantseva, and A. F. Starace, *J. Phys. B* **42**, 035601 (2009).
- [28] G. Vampa, C. R. McDonald, G. Orlando, D. D. Klug, P. B. Corkum, and T. Brabec, *Phys. Rev. Lett.* **113**, 073901 (2014).
- [29] P. G. Hawkins, M. Y. Ivanov, and V. S. Yakovlev, *Phys. Rev. A* **91**, 013405 (2015).
- [30] T. Higuchi, M. I. Stockman, and P. Hommelhoff, *Phys. Rev. Lett.* **113**, 213901 (2014).
- [31] M. Wu, S. Ghimire, D. A. Reis, K. J. Schafer, and M. B. Gaarde, *Phys. Rev. A* **91**, 043839 (2015).
- [32] Z. Guan, X.-X. Zhou, and X.-B. Bian, *Phys. Rev. A* **93**, 033852 (2016).
- [33] T.-Y. Du, D. Tang, X.-H. Huang, and X.-B. Bian, *Phys. Rev. A* **97**, 043413 (2018).
- [34] F. Navarrete, M. F. Ciappina, and U. Thumm, *Phys. Rev. A* **100**, 033405 (2019).

- [35] J. Li, S. Fu, H. Wang, X. Zhang, B. Ding, B. Hu, and H. Du, *Phys. Rev. A* **98**, 043409 (2018).
- [36] J. Ma, C. Zhang, H. Cui, Z. Ma, and X. Miao, *Chem. Phys. Lett.* **744**, 137207 (2020).
- [37] T. T. Luu and H. J. Wörner, *Phys. Rev. B* **94**, 115164 (2016).
- [38] S. Jiang, J. Chen, H. Wei, C. Yu, R. Lu, and C. D. Lin, *Phys. Rev. Lett.* **120**, 253201 (2018).
- [39] I. Floss, C. Lemell, G. Wachter, V. Smejkal, S. A. Sato, X.-M. Tong, K. Yabana, and J. Burgdörfer, *Phys. Rev. A* **97**, 011401(R) (2018).
- [40] N. Tancogne-Dejean, O. D. Mücke, F. X. Kärtner, and A. Rubio, *Phys. Rev. Lett.* **118**, 087403 (2017).
- [41] D. Bauer and K. K. Hansen, *Phys. Rev. Lett.* **120**, 177401 (2018).
- [42] C. Yu, K. K. Hansen, and L. B. Madsen, *Phys. Rev. A* **99**, 063408 (2019).
- [43] R. E. F. Silva, I. V. Blinov, A. N. Rubtsov, O. Smirnova, and M. Ivanov, *Nat. Photonics* **12**, 266 (2018).
- [44] D. T. Colbert and W. H. Miller, *J. Chem. Phys.* **96**, 1982 (1992).
- [45] K. K. Hansen, T. Deffge, and D. Bauer, *Phys. Rev. A* **96**, 053418 (2017).
- [46] K. K. Hansen, D. Bauer, and L. B. Madsen, *Phys. Rev. A* **97**, 043424 (2018).
- [47] S. Minemoto, T. Umegaki, Y. Oguchi, T. Morishita, A.-T. Le, S. Watanabe, and H. Sakai, *Phys. Rev. A* **78**, 061402(R) (2008).
- [48] A. D. Shiner, B. E. Schmidt, C. Trallero-Herrero, H. J. Wörner, S. Patchkovskii, P. B. Corkum, J.-C. Kieffer, F. Légaré, and D. M. Villeneuve, *Nat. Phys.* **7**, 464 (2011).
- [49] J. Higuier, H. Ruf, N. Thiré, R. Cireasa, E. Constant, E. Cormier, D. Descamps, E. Mével, S. Petit, B. Pons, Y. Mairesse, and B. Fabre, *Phys. Rev. A* **83**, 053401 (2011).
- [50] K. Uchida, V. Pareek, K. Nagai, K. M. Dani, and K. Tanaka, *arXiv:2006.09376*.
- [51] H. Irvani, K. K. Hansen, and L. B. Madsen, *Phys. Rev. Research* **2**, 013204 (2020).
- [52] M. S. Mrudul, N. Tancogne-Dejean, A. Rubio, and G. Dixit, *npj Comput. Mater.* **6**, 10 (2020).
- [53] A. Pattanayak, M. S. Mrudul, and G. Dixit, *Phys. Rev. A* **101**, 013404 (2020).
- [54] G. Orlando, T.-S. Ho, and S.-I. Chu, *J. Opt. Soc. Am. B* **37**, 1540 (2020).